IJCRT.ORG ISSN : 2320-2882

INTERNATIONAL JOURNAL OF CREATIVE RESEARCH THOUGHTS (IJCRT)

An International Open Access, Peer-reviewed, Refereed Journal

Porous Shiitake Mushroom Carbon Composite With $Nico_2o_4$ Nano-Rod Electrochemical Characteristics For Efficient Supercapacitor Applications

Balamuralitharan Balakrishnan,[*a]

[a] Department of Electronics and Communication Engineering, Vel Tech Rangarajan Dr. Sagunthala R&D Institute of Science and Technology, Chennai, 600062 Tamil Nadu, India

A new composite electrode based on m-C/NiCo2O4 nanorod arrays (NRAs), which improves the pseudo capacitive properties by effectively amplifying the electrochemical performance for applications of supercapacitor. Carbon or graphene based nanorod thin films have been used in supercapacitors with gravimetric capacitances of (85–250 F/g), but areal specific capacitance of (5–60 mF/cm2) is low due to the thickness and low mass loading, which is undesirable for practical applications. The present study, shitake mushroom was used as the carbon precursor. The shiitake mushroom provides a higher surface area and higher energy storage value compared to other carbon materials. m-C/NiCo2O4 composite made of NiCo2O4 nanorod combined with carbon made from shitake mushroom using hydrothermal method, provides a higher specific capacitance when compared to other composite and carbon electrodes. The formation of m-C/NiCo2O4 composite nanorods attributes to the higher surface area for the ions which resulted in a high specific capacitance. Porous properties of natural carbon and NiCo2O4 metal oxides effectively amplified the capacitance behavior and enhances stability. The structures and electrochemical behavior of the samples are examined with Scanning electron microscopy, X-ray diffraction, X-ray photon spectroscopy, EDAX , cyclic voltammetry, galvanostatic charge –discharge and impedance spectra respectively. Therefore, the specific capacitance, excellent cycling stability with extraordinary mechanical flexibility is been improved using m-C with a high surface area combined with NiCo2O4. m-C/NiCo2O4 coin cell showed higher stability and energy storage capacity (556 F/g at current density of 10 A/g). The cause for increase in capacitance and structural behavior and the effect of electrochemical performance are been investigated and discussed.

Introduction

The rapid growth in technology and fuel consumption over the past few decades has led to a high demand for energy storage. The demand for other bio-friendly and renewable energy sources will reduce the dependence on fossil fuels, and has prompted the development of storage technologies.[1][2] Although the technologies of harvesting renewable energy, such as lithium-ion battery technology , fuel cells, perovskites and dye-sensitized solar cells,[3–6] significantly improved over time, more techniques to produce, store, and deliver the generated energy are needed. The properties of supercapacitors lies in between conventional capacitors and batteries, and have been studied globally as a promising method as the energy storage devices for next-generation technology owing to their remarkable properties, such as higher power densities, long cycling stability, and fast charge/discharge processes.[7] In supercapacitors, faradic charge transfer plays a major role and needs to be considered when choosing the appropriate material for efficient supercapacitors. This faradaic charge transfer arises by a very prompt sequence of reversible faradaic redox, electro-adsorption or intercalation processes of the appropriate electrode surfaces.[8] Owing to its large surface area, prominent catalyst for transfer of electrons, intercalation, excellent electrical conductivity and sufficient heat resistant property makes carbon based materials as the significant electrode materials for supercapacitor applications.[9] Electrochemical capacitors (ECs), also called supercapacitors, are fast-developing high-performance electrical energy storage devices which receive enormous research attention worldwide.[10] Supercapacitors store and release energy based on either the accumulation of charges at the interface between electrolyte and electrode (double layer capacitors) or redox reactions take place at the surface of the electroactive material (pseudocapacitor) or both (hybrid electrochemical capacitors).[11]

The carbonization of natural materials is a cost-effective route for the scalable production of Activated Carbon for applications in waste water treatment,[12] biosensors,[13] and energy storage.[14–20] Thus far, various natural products have been used as the carbon alternatives in the field of supercapacitors to produce good morphological structures and higher capacity storage.[21] The morphology of natural carbon plays a key role in increasing the power density and energy density of the capacitors. For example, the carbonization of watermelon yield a chemically active and physically flexible carbon aerogel, which excellently scaffolds with Fe_3O_4 nanoparticles for pseudocapacitor applications.[22] The bamboo sticks in alkaline solution which had been treated hydrothermally was been carbonized as carbon fibers, which exhibited enhanced capacitive performance when made as the composite with MnO_2.[23] Most recently, chitin-protein fibers mineralized in crab shells were used as biotemplate for Li-ion batteries and supercapacitors.[24, 25] Plant biomass, including banana peels, Lettuce leaves and Typha orientalis have also been effectively deployed as carbon products.[26]

Their pore sizes and distribution of pores in a carbon material plays vital role in good capacitive performance.[27] ACs used in the current in current studies composed primarily of micro-pores less than

2.0 nm in size. Such structural limitations result in a higher diffusion resistance, leading worse retention of capacity and to poor charge storage. To meet the requirements of high storage capacity and high conductivity, the meso and nano pores carbon material having lesser distance between the pores in needed.[28][29] The pores usually serve as ion buffer reservoirs shortening ion diffusion length, when micro- and mesopores are essential for improving the charge storage ability, leading to achieve both high power density and high energy density. Carbon-based materials with a high surface area are usually used as electrodes in this type of supercapacitors.[30] The present study shows, shitake mushroom was used as the carbon precursor. The shiitake mushroom provides a higher surface area and higher energy storage value compared to other carbon materials. Ping Cheng et al. proving that shiitake mushrooms have higher capacitive storage than other natural carbons.[31] In oxide materials, NiCO2O4 has higher capacitance than MnO2 and Fe3O4.[32][33][34] Many reported work have suggested that depositing pseudocapacitance materials on conductive network (current collector) facilitates to enhance the conductivity of electrodes composed of pseudocapacitance materials.[35] By combining the shiitake mushroom carbon with NiCo2O4, a novel composite material was synthesized for high capacitance and higher stability than that reported thus far according to the authors' knowledge.[36] This paper presents the synthesis of m-C/NiCo2O4 composite material via a hydrothermal reaction involving the preparation of a highly porous activated carbon using the shiitake mushroom. The material characterization, studies using this composite material using shitake mushroom carbon proves to be more efficient than the other carbon composite with NiCo2O4.[37]

2. Experimental section

2.1 Synthesis Procedure

Edible shiitake mushroom, several grams in mass, was cleaned in distilled water and kept in a crucible. The mushroom was dried at 80° C for 12hrs. After cooling, mushroom was soaked in $(NH_4)_2HPO_4$ solution (7.5%) at room temperature for 3 hours and kept in oven at 80° C for 12hrs. The resultant dried mushroom was then carbonized at 500° C for 5hrs. After carbonization of m-C, it was activated by heating it in CO_2 atmosphere at 1000°C for 2hrs. The derived sample of m-C (0.15g) was mixed with 0.3 g of $NiCl_2.6H_2O$ and 0.6 g of $CoCl_2.6H_2O$ in 10ml double distilled water. The solution was stirred well. Then 30ml of methanol and 5.4 g of urea was been added to the stirred solution. After 15 min of stirring, the clear pink colored solution was subjected into an autoclave having Teflon liner and was heated to 120°C for 6hrs, forming a purple color solution. The solution was thoroughly washed numerous times with ethanol to remove the unreacted impurities. Then, the obtained mixture was centrifuged and the sediment was heated at 60°C for drying. After drying composite powder of m-C/NiCo2O4 yielded. Then the yield is annealed for 300°C.

$NiCo2O4 + OH- + H2O \rightleftharpoons NiOOH + 2CoOOH + e-$ (1)

2.2 Physico-Chemical characterization

The synthesized sample's crystallinity was studied using X-ray diffraction (XRD) pattern with D8 ADVANCE diffractometer. The conditions were using Cu Kα radiation having 40kv-40mA further accompanied by 2θ range from 20-80°.

Microstructures and the surface morphology of the obtained materials were characterized by Field Emission scanning electron microscopy (FE-SEM) technique by Hitachi S-4200 with EDX. X-ray photoelectron spectroscopy (XPS) measurements were analysed by VG Scientific – ESCALAB 250 equipped with Al-Kα X-ray excitation.

2.3 Electrochemical measurement

The electrochemical measurements were carried out using three compartment electrode system consisting of working electrode, counter electrode and reference electrode with alkaline electrolyte (6 M KOH) at room temperature. The saturated Ag/AgCl electrode immersed in KCl solution and Platinum wire used as the reference electrode and counter electrode respectively, for this study. In order to prepare working electrode, $NiCo_2O_4$ and m-C/$NiCo_2O_4$ nanocomposites coated on nickel foam by mixing with 5 wt. % PVDF binder and 10 wt. % of carbon black. Cyclic voltammogram (CV) was studied with varying the sweep rates (5, 20, 50 and 100 mV s^{-1}) between the potential window of 0.1 and 0.4 V. The GCD (galvanostatic charge-discharge) test was studied with different current densities of 10, 20, 30 and 40 A g^{-1}. EIS (Electrochemical impedance spectroscopy) was studied in a frequency range of 100 kHz. To make the coin cell device, m-C/$NiCo_2O_4$ was assembled into symmetrical electrodes by mixing with 5 wt. % PVDF binder and 10 wt. % of carbon black. The mixture was homogenized in an agate mortar, spread over copper foil and left to stand at 70°C for 24 hrs. The dried product was punched out as 1.6 cm diameter disks. A coin cell was assembled with a spacer having the counter electrode in one side and the anode in other. The separator, Millipore glass fiber was placed in between the counter electrode and anode. A 6M KOH added to distilled water to prepare electrolyte solution and the coin cell was sealed and tested. Cyclic voltammogram (CV) and CD was studied with varying the sweep rates (5, 20, 50 and 100 mV s-1) between the potential window of 0.1 and 0.4 V. The weight of the material coated in coin cell is 1mg.

3. Results and Discussion

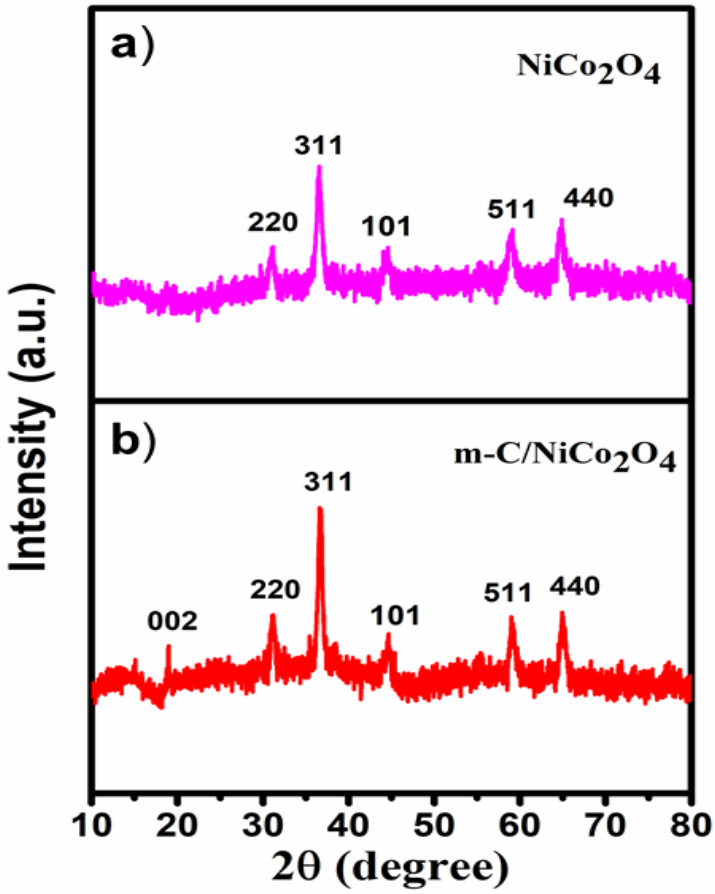

Fig 1. a) & b) XRD pattern of the working electrodes.

X-ray diffraction (XRD) having diffraction peaks showing crystalline NiCo2O4 and m-C/ NiCo2O4 in Fig 1. The JCPDS data no. 20-0781 shows the hkl planes of 220, 311, 400, 511, and 440 in figure 1b showing the NiCo2O4 diffraction peaks and figure 1b having JCPDS no. 73-1702 shows extra 002 and 101 hkl planes corresponding to the carbon material which confirms the presence of carbon in the composite in m-C/ NiCo2O4. The crystalline nature of the material absorbs the broad peaks, which indicated a size of approximately 100nm in width and 700nm in length and using Scherer's equation the average crystalline size is to be calculated around 130 nm.

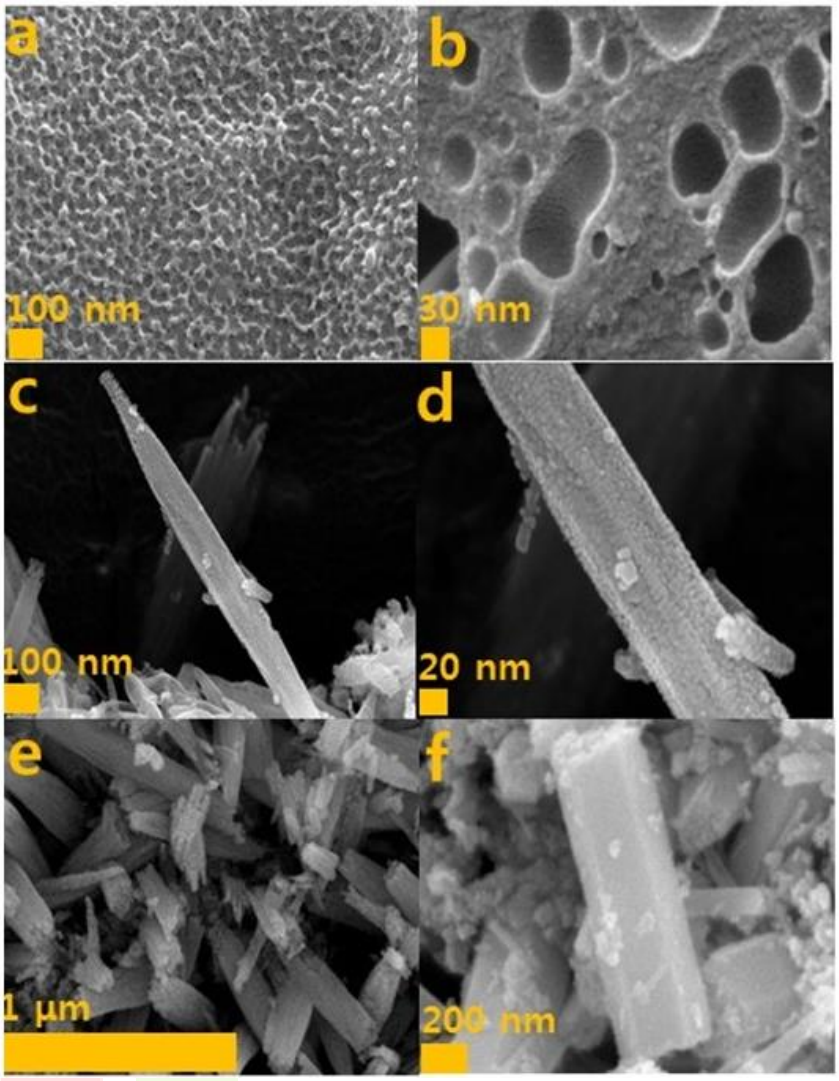

Fig 2. a) and b) shows the porous nature of mushroom carbon, c), d) and e) FE-SEM images of a porous m-C/$NiCo_2O_4$ composite nanorods and f) Crystalline structure of non-composite $NiCo_2O_4$ nanorod.

Fascinatingly, the hydrothermal reaction influences to change nano particles morphology structure. This method makes this m-C/$NiCo_2O_4$ to form nano rod structure. Nano rod structure can be clearly seen in the FESEM of the m-C/$NiCo_2O_4$ and $NiCo_2O_4$ samples (Fig. 2 (a) and (b)). The FESEM also reveals that the porous nature of the mushroom carbon, whereas in composites (Fig. 2 (c), (d) and (e)) shows the m-C/$NiCo_2O_4$ material formed as nanorods without any distinctive or remarkable changes in structures due to the involvement of mesoporous carbon material, which strongly adhered as the composite to $NiCo_2O_4$. On the other hand, $NiCo_2O_4$ had a hexagonal crystal grain structure formation was clearly illustrated in Fig. 2 (f). The effect of carbon clearly implies on NiCo2O4 when seen in the figures. The average size of the m-C/NiCo2O4 is approximately width of

80nm to 240nm and length of 700nm. This nanorod structures helps in the quantity of reactive area and porous nature helps in increasing electric conductivity and large surface area to store ions. [11, 38]

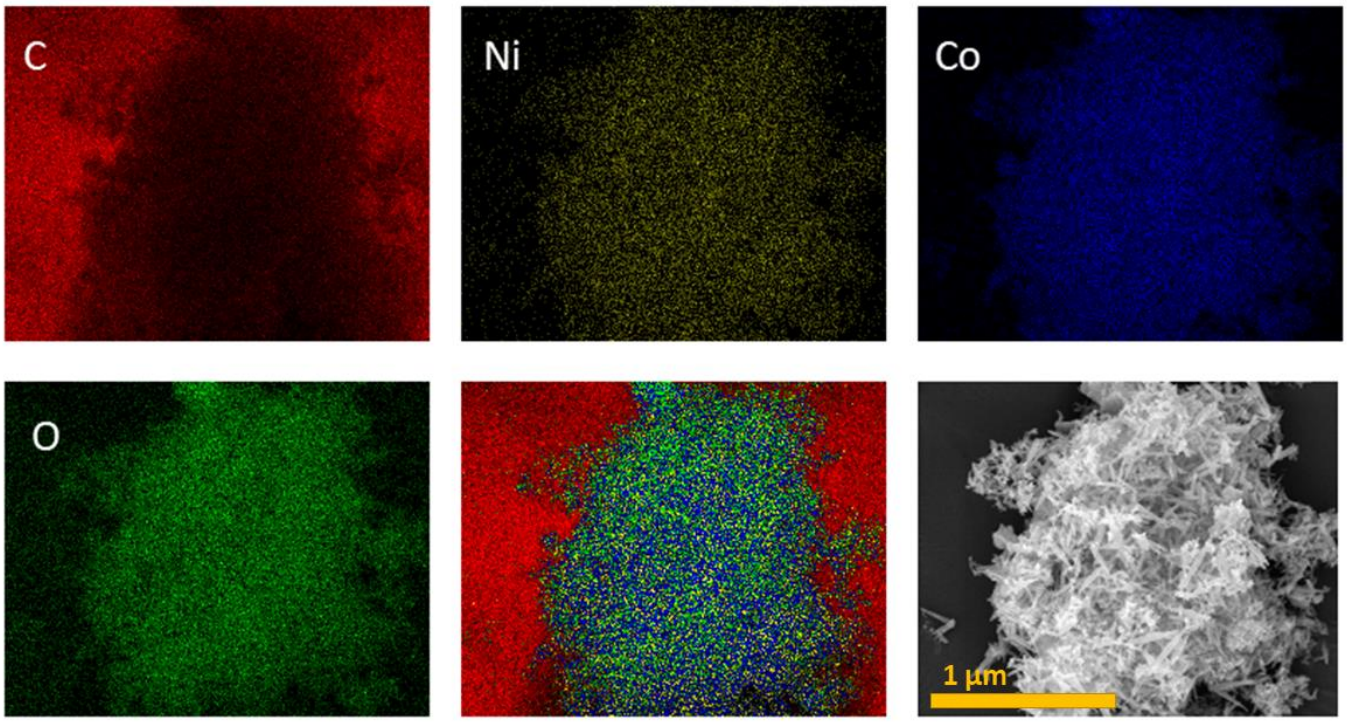

Fig 3: EDX mapping images of various material in m-C/ $NiCo_2O_4$ nanorods.

EDX mapping further proves the existence of O, Ni, C and Co in the synthesized material, as shown in Fig 3. The oxygen presence results in formation of oxides. The chemical composition was further verified by XPS in Fig. 4. The spectra revealed that the existence of C, Ni, Co, and O. The carbon, C 1s spectrum showed peaks for C-C, C-O and C=O with the corresponding binding energies of 284.56, 286.04, and 288.48 eV respectively. Peaks for Ni 2p3/2 and Ni 2p1/2 was observed at 854.82 eV (Ni2+) and 856.31eV (Ni3+), and 871.89 eV (Ni2+) and 874.05 eV (Ni3+), respectively.[39, 40] Furthermore, peaks for Co 2p3/2 and Co 2p1/2 were noted at 779.96 eV (Co2+) and 795.09 eV (Co2+), respectively, was depicted in Fig 4 (c).[41] The binding energies for Co 2p3/2 and Co 2p1/2 (Co3+) were 781.51 eV and 796.78 eV, respectively. The three peaks for oxygen (O1, O2 and O3) implies: O1 at 529.82 eV on O spectrum, indicating metal oxygen; the peak for O2 at 531.58 eV for oxygen ions; and the peak for O3 at 533.26 eV indicating chemisorbed oxygen within the surface and under-coordinated lattice oxygen.[42, 43]

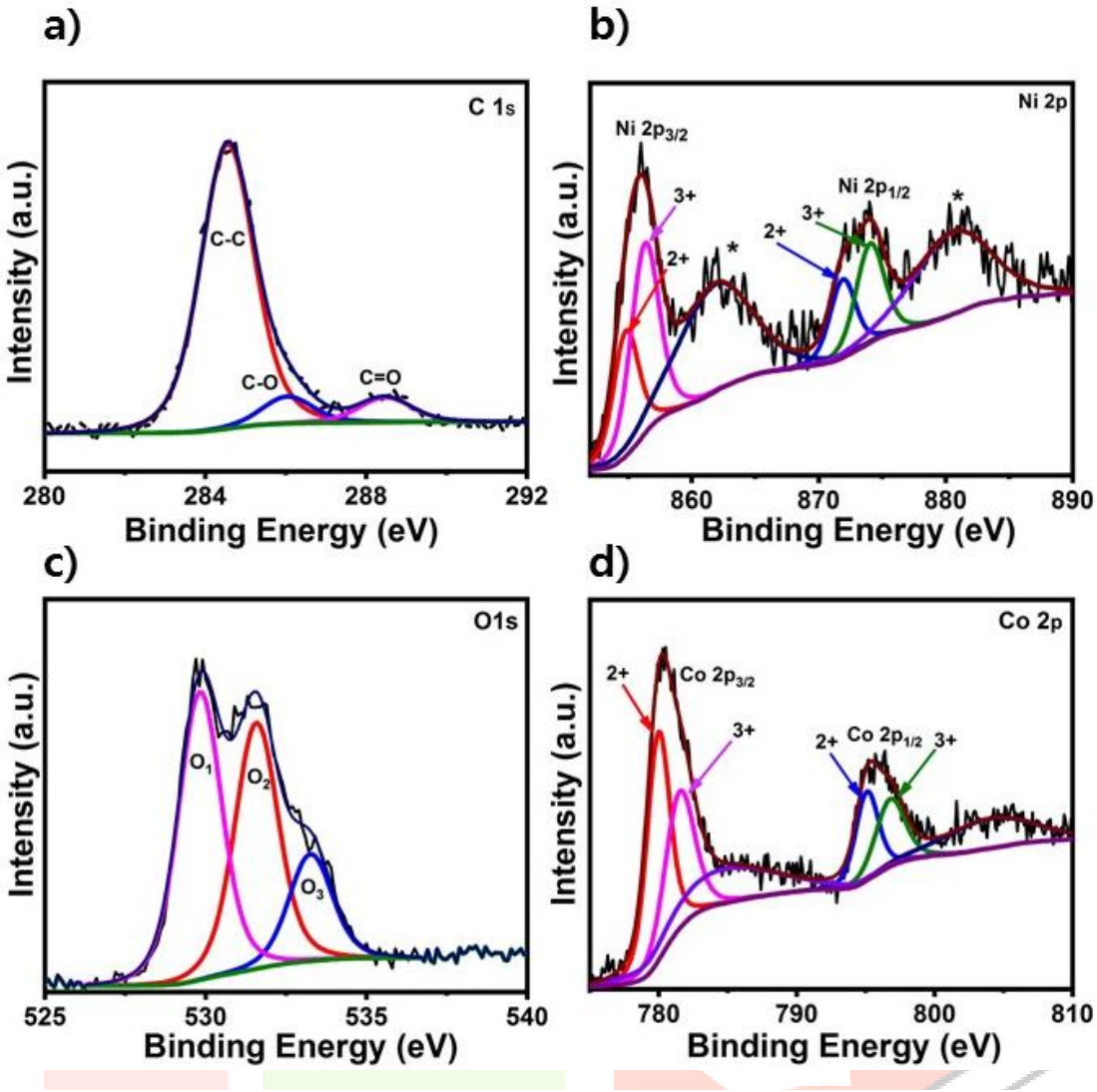

Fig 4. XPS spectra of (a) C1s, (b) Ni 2p, (c) Co 2p and (d) O 1 s regions of m-C/ NiCo2O4

The electro chemical behavior m-C/ $NiCo_2O_4$ and $NiCo_2O_4$ was investigated using three electrode system shown in fig 5. In contrast, due to the presence of m-C in $NiCo_2O_4$, m-c/$NiCo_2O_4$ shows good capacitance value than unaltered $NiCo_2O_4$. m-C/ $NiCo_2O_4$ capacitance shows 3517.76 F g^{-1}, 2001.03 F g^{-1}, 1020.21 F g^{-1}, and 738.53 F g^{-1} at various scan rates. Unaltered $NiCo_2O_4$, exhibits specific capacitance of 2014.82 F g^{-1}, 1123.21 F g^{-1}, 791.56 F g^{-1}, and 512.42 F g^{-1} at different scan rates. The results denotes that the m-C with large surface area makes the difference in m-C/$NiCo_2O_4$. This was described clearly to the high surface area of m-C, which allows the ions to settle down in highly porous framework of the m-C. The shape of the CV curves with bulge showing that oxidation and reduction peaks are present which implies redox reaction taking place prominently, certainly also in higher scan rates. The peaks current increased with increasing the sweep rate when the oxidation and reduction peak shift towards higher and lower potentials respectively. This process leads to the fast movement of ions inter and intra surface of the electrode. The redox peaks can be attributed mainly to the redox reactions linked to N-O/N-O-OH (N represents Ni or Co). Moreover the solid state redox couples of Co^{2+}/Co^{3+} and Ni^{2+}/ Ni^{3+} having to different types of active centers

are present in the structure, there were no couple redox peaks of Ni^{2+}/ Ni^{3+} and Co^{2+}/Co^{3+}due to the comparable redox potential due to the surface modification of $NiCo_2O_4$ composite with m-C. A comparison of the voltammograms of $NiCo_2O_4$ and m-C/ $NiCo_2O_4$ revealed a difference in both CV curves; m-C/ $NiCo_2O_4$ showed a stronger redox reaction than $NiCo_2O_4$. The excellent behavior of m-C/$NiCo_2O_4$ resulted mainly due to the reversible adsorption of ions present in the electrolyte rather than $NiCo_2O_4$. This totally depends on the porous nature of the m-C composite with $NiCo_2O_4$. The m-C provided a highly conductive support for $NiCo_2O_4$, resulting in a better rate capability.

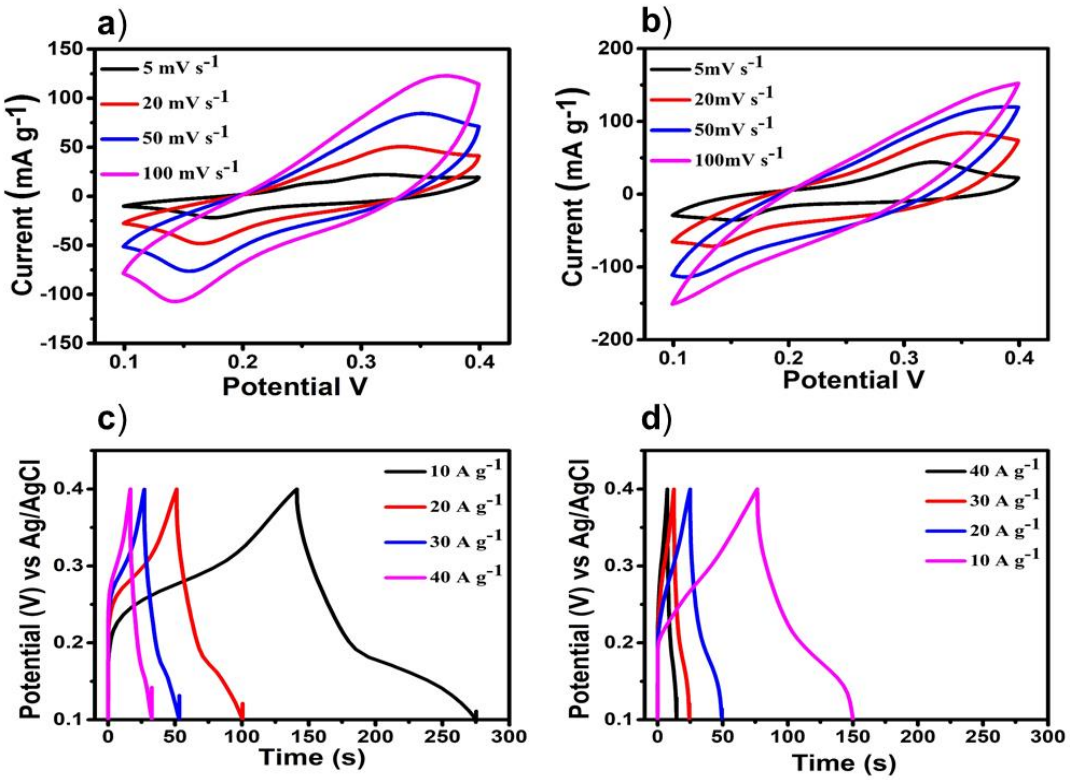

Fig 5. Electro chemical performance of m-C/$NiCo_2O_4$ and $NiCo_2O_4$. a) and b) CV curves of m-C/$NiCo_2O_4$ and $NiCo_2O_4$ respectively. c) and d) shows the CD curves of m-C/$NiCo_2O_4$ and $NiCo_2O_4$ respectively.

According to galvanometric charge-discharge investigation, the capacitance for m-C/ NiCo2O4 was 4148, 3219, 2153, and 1543 Fg−1 at specified current densities respectively and specific capacitance of NiCo2O4 was 2434, 1613, 1228 and 914 Fg-1. These values clearly shows m-C/ NiCo2O4 having upper hand over NiCo2O4, confirming m-C supports NiCo2O4 enhancing performance. The decrease in specific capacitance at high current densities (≥ 40 A g-1) described to the low diffusion of ions in the supporting electrolyte. Salunkhe et al.[44] reported nickel cobaltite material using CBD technique having specific capacitance of 490 Fg−1. Kuang et al.[45] reported NiCo2O4 by a hydrothermal technique having capacitance of 372 Fg−1. Nickel–cobalt hydroxide by CBD technique having capacitance of 456 Fg−1, Salunkhe et al.[46] The reported specific capacitance shown in higher capacitance is due to the porous nature and nanorod

morphology. The cyclic voltammetry of the symmetrical cell revealed a lower specific capacitance compared to the three electrodes tested. In real-time applications, a two electrode system is taken into account. The coin cell revealed a higher specific capacitance of 515 F/g at a scan rate of 5mV/s. The capacitance decreased with increasing scan rate. The diffusion of ions exists predominantly in the outer regions of the pores at higher scan rates, while both inner and outer surfaces could easily facilitated by the ions in the electrolyte at lower scan rate, which demonstrates the high specific capacitance of the material at a lower sweep rate.[47] In fig 6 (b) shows the CD curve of the electrode material exhibited pseudocapacitance behavior. The charge-discharge curve in Fig 6 b) showed a maximum capacitance of 578.67 F/g at a current density of 10A/g. When compared to the current density at 10A/g, the discharge time at a 20 and 30A/g current density was shorter than that at 10A/g. YuOuyang et al, prepared CC/NiCo2O4 asymmetric cell showed lower specific capacitance when compared to m-C/NiCo2O4.[48] The derived specific capacitances decreases with increase in current density. It is mainly due to the lack of time availability at larger current densities for the efficient movement of K+ ions into the bulk portions of the electrode, which hinders the existence of re-dox reactions to the outer surface of the electrode.[49] The cycling stability of the m-C/ NiCo2O4-based coin cell electrode was measured for 3000 cycles. The coin cell electrode material retained approximately 84% of its initial capacitance at the current density of 10A/g. In fig 6 C), the cycling stability of the m-C/ NiCo2O4-based three electrode system was measured for 3000 cycles, and there was a steady decrease in specific capacitance of the electrode material. The electrode retained approximately 86% of its initial capacitance at 10 A/g until the 3000th cycle. Therefore, the electrode material shows excellent long-term stability and is suitable for real-time applications. The degradation of the electrode material was minimal at the 3000th cycle due to the doping of carbon with NiCo2O4. The coin cell electrode showed 84% high retention in the cycling stability test when compared to other works.[48] The materials performance improves by electrode wetting with the electrolyte, making way to electroactive surface area. The surface area of the m-C plays a major role in the storage of more ions compared to $NiCo_2O_4$.[50] Therefore, m-C/ $NiCo_2O_4$ has better cycling stability than $NiCo_2O_4$. In contrast to the coin cell electrode, the retention percentage of the initial capacitance was similar to the m-C/ $NiCo_2O_4$-based three-electrode system. There is no significant difference in retention rate, highlighting its great stability for commercial uses.

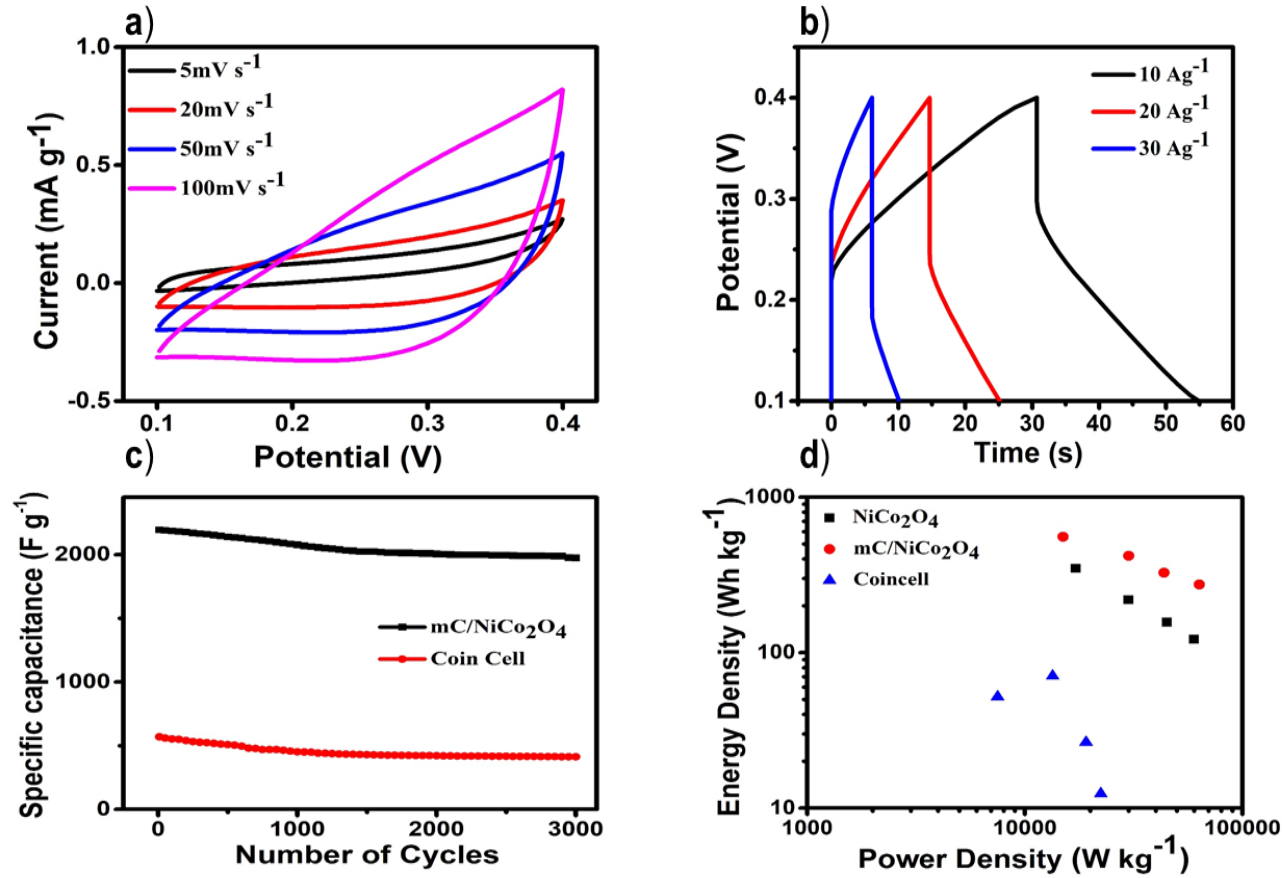

Fig 6. a) Coin cell m-C/$NiCo_2O_4$ CV curves, b) coin cell m-C/ $NiCo_2O_4$ electrode Charge-Discharge curves, c) Cycling performance of coin cell m-C/$NiCo_2O_4$ and m-C/$NiCo_2O_4$ during 3000 cycles and d) m-C/ $NiCo_2O_4$ Ragone plot.

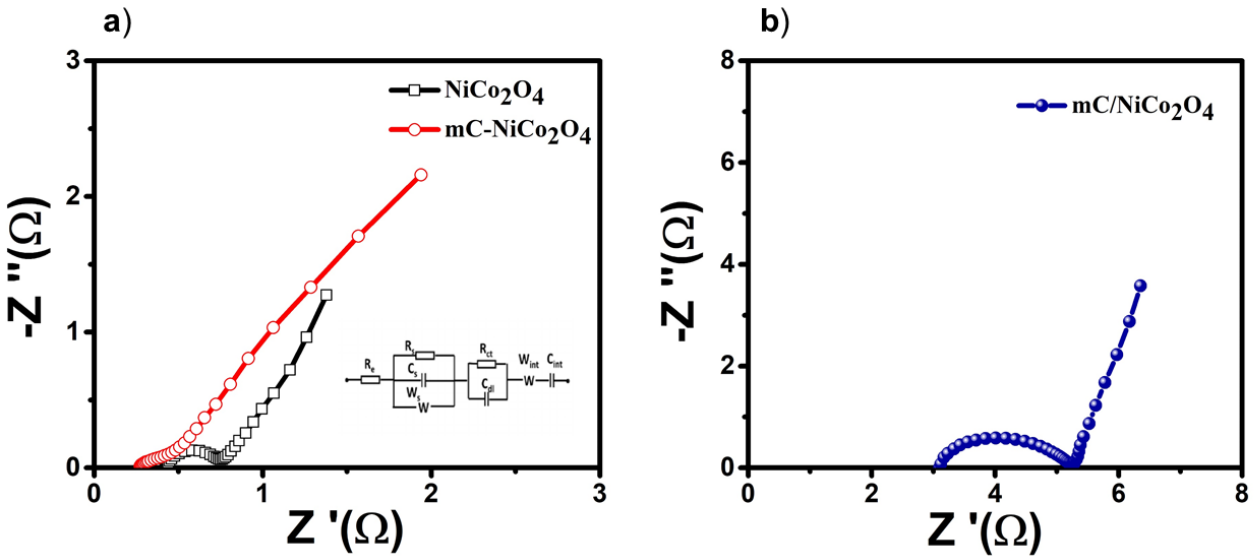

Fig 7. a) m-C/ $NiCo_2O_4$ and $NiCo_2O_4$ electrode's Nyquist plot and b) m-C/ $NiCo_2O_4$ coin cell electrode's Nyquist plot.

Electrodes tested in the 6 M KOH having frequency range of 100 kHz. The EIS was consists of a single semicircle at higher frequency and followed by a linear component at lower frequency. In the lower frequency region, Warburg resistance (ZW) was shown at the slope of the curve, indicating electrolyte diffusion on the surface of the electrode. The semicircle in the low frequency

region of m-C/ $NiCo_2O_4$ curve is not noticeable compared to $NiCo_2O_4$. The increased capacitive performance at lower current density, attributes to the superior performance of the electro active surface compared to $NiCo_2O_4$. The pore size allows better storage of the charge due to the introduction of m-C in $NiCo_2O_4$. In m-C/$NiCo_2O_4$, the pores acts as an ion-buffering reservoir, which promotes a faster permeation into the electrolyte, reducing the diffusion distance of OH^-, which helps the insertion and extraction of possible OH^- ions. Fig 7 b) exhibits the resistance of the coin cell m-C/ $NiCo_2O_4$ electrode in a Nyquist plot. The impedance spectra were similar; they were composed of a semicircle component at the high frequency range and a linear component at the low frequency range. The ionic resistance of the electrolyte is the sum of internal resistance, such as intrinsic resistance of the active material, and the contact resistance at the active material side and current collector side. The semicircle ranged from approximately 5.3Ω and the overall resistance at the highest peak was approximately 5.8Ω, indicating negligible resistance in the coin cell electrode. Therefore, the conductivity and OH- ion transfer were greater in the coin cell electrode. The obtained results clearly illustrate that the combination of low electron transfer resistance and rapid ion diffusion synergistically increase the electrochemical performance of the coin cell m-C/ NiCo2O4 electrode. The energy density and maximum power density of the symmetric device and the electrode materials were calculated from the CP curves at different current densities respectively. The Ragone plot showed that the symmetric cells had the highest energy density of 52.083 Wh kg-1 and maximum power density of 7499.52 W kg-1 at a current density of 5 A/g. The calculated power density was higher than that reported in other studies, such as the Carbon composite with NiCo2O4 for symmetric cell[51] porous NiCo2O4 for a symmetric cell[43], CNT/ graphene composite[52], and RGO/Acetylene black[53] . Therefore, this material is suitable for commercial applications.

4. Conclusions

From the obtained results, m-C/$NiCo_2O_4$ possesses excellent electrode material for supercapacitor application by a simple and effective hydrothermal synthesis method. The $NiCo_2O_4$ nanorod morphology was changed due to the implementation of m-C in the surface. The electro chemical properties of m-C/$NiCo_2O_4$ is superior due to the porous nature, morphology of the composite material and the large surface are of the carbon based on shitake mushroom. The long term stability is also obtained in m-C/$NiCo_2O_4$ against the $NiCo_2O_4$. The coil cell device, which was fabricated from the m-C/$NiCo_2O_4$ electrode material, showed lower capacitance than the m-C/$NiCo_2O_4$ three electrode system but had higher stability compared to other composite materials. Overall, the m-C/$NiCo_2O_4$ electrode has good potential for commercial applications.

Acknowledgements

The authors gratefully acknowledge the support from Basic Research Laboratory through the National Research Foundations of Korea funded by the Ministry of Science, ICT and Future Planning (NRF-2015R1A4A1041584). The authors would like to thank KBSI, Busan for instrumentation facility.

References

1. Augustyn V, Simon P, Dunn B (2014) Pseudocapacitive oxide materials for high-rate electrochemical energy storage. Energy Environ Sci 7:1597–1614. https://doi.org/10.1039/c3ee44164d

2. Zhou E, Wang C, Shao M, et al (2017) MoO2 nanoparticles grown on carbon fibers as anode materials for lithium-ion batteries. Ceram Int 43:760–765. https://doi.org/10.1016/j.ceramint.2016.10.006

3. Wang X, Cao X, Bourgeois L, et al (2012) N-doped graphene-SnO 2 sandwich paper for high-performance lithium-ion batteries. Adv Funct Mater 22:2682–2690. https://doi.org/10.1002/adfm.201103110

4. Li W, Gan L, Guo K, et al (2016) Self-supported Zn3P2nanowire arrays grafted on carbon fabrics as an advanced integrated anode for flexible lithium ion batteries. Nanoscale 8:8666–8672. https://doi.org/10.1039/c5nr08467a

5. Yao N, Huang J, Fu K, et al (2014) Efficiency enhancement in dye-sensitized solar cells with down conversion material ZnO: Eu3+, Dy3+. J Power Sources 267:405–410. https://doi.org/10.1109/ICPP.2015.93

6. Simon P, Gogotsi Y (2008) Materials for electrochemical capacitors. Nat Mater 7:845

7. Wang Y, Song Y, Xia Y (2016) Electrochemical capacitors: Mechanism, materials, systems, characterization and applications. Chem Soc Rev 45:5925–5950. https://doi.org/10.1039/c5cs00580a

8. Abruña HD, Kiya Y, Henderson JC (2008) Batteries and electrochemical capacitors. Phys Today 61:43–47. https://doi.org/10.1063/1.3047681

9. Fialkov AS (2000) Carbon application in chemical power sources. Russ J Electrochem 36:345–366. https://doi.org/10.1007/BF02756940

10. Wang B, Zhu T, Wu H Bin, et al (2012) Porous Co<inf>3</inf>O<inf>4</inf> nanowires derived from long Co(CO <inf>3</inf>)<inf>0.5</inf>(OH)·0.11H<inf>2</inf>O nanowires with improved supercapacitive properties. Nanoscale 4:2145–2149. https://doi.org/10.1039/c2nr11897a

11. Balamuralitharan B, Cho IH, Bak JS, Kim HJ (2018) V2O5nanorod electrode material for enhanced electrochemical properties by a facile hydrothermal method for supercapacitor applications. New J Chem 42:11862–11868. https://doi.org/10.1039/c8nj02377h

12. Liu RL, Liu Y, Zhou XY, et al (2014) Biomass-derived highly porous functional carbon fabricated by

using a free-standing template for efficient removal of methylene blue. Bioresour Technol 154:138–147. https://doi.org/10.1016/j.biortech.2013.12.034

13. Gong C, Chen J, Song Y, et al (2016) A glucose biosensor based on the polymerization of aniline induced by a bio-interphase of glucose oxidase and horseradish peroxidase. Anal Methods 8:1513–1519. https://doi.org/10.1039/c5ay02762d

14. Wang L, Zheng Y, Zhang Q, et al (2014) Template-free synthesis of hierarchical porous carbon derived from low-cost biomass for high-performance supercapacitors. RSC Adv 4:51072–51079. https://doi.org/10.1039/c4ra07955h

15. Chen P, Wang LK, Wang G, et al (2014) Nitrogen-doped nanoporous carbon nanosheets derived from plant biomass: An efficient catalyst for oxygen reduction reaction. Energy Environ Sci 7:4095–4103. https://doi.org/10.1039/c4ee02531h

16. Qian W, Sun F, Xu Y, et al (2014) Human hair-derived carbon flakes for electrochemical supercapacitors. Energy Environ Sci 7:379–386. https://doi.org/10.1039/c3ee43111h

17. Gao S, Chen Y, Fan H, et al (2014) Large scale production of biomass-derived n-doped porous carbon spheres for oxygen reduction and supercapacitors. J Mater Chem A 2:3317–3324. https://doi.org/10.1039/c3ta14281g

18. Hong KL, Qie L, Zeng R, et al (2014) Biomass derived hard carbon used as a high performance anode material for sodium ion batteries. J Mater Chem A 2:12733–12738. https://doi.org/10.1039/c4ta02068e

19. Ren Y, Zhang J, Xu Q, et al (2014) Biomass-derived three-dimensional porous N-doped carbonaceous aerogel for efficient supercapacitor electrodes. RSC Adv 4:23412–23419. https://doi.org/10.1039/c4ra02109f

20. Ruan C, Ai K, Lu L (2014) Biomass-derived carbon materials for high-performance supercapacitor electrodes. RSC Adv 4:30887–30895. https://doi.org/10.1039/c4ra04470c

21. Raman V, Punnoose D, Baraneedharan P, et al (2017) Study on the efficient PV/TE characteristics of the self-assembled thin films based on bismuth telluride/cadmium telluride. RSC Adv 7:. https://doi.org/10.1039/c6ra26638j

22. Wu XL, Wen T, Guo HL, et al (2013) Biomass-derived sponge-like carbonaceous hydrogels and aerogels for supercapacitors. ACS Nano 7:3589–3597. https://doi.org/10.1021/nn400566d

23. Jiang J, Zhu J, Ai W, et al (2014) Evolution of disposable bamboo chopsticks into uniform carbon fibers: A smart strategy to fabricate sustainable anodes for Li-ion batteries. Energy Environ Sci 7:2670–2679. https://doi.org/10.1039/c4ee00602j

24. Yao H, Zheng G, Li W, et al (2013) Crab shells as sustainable templates from nature for nanostructured battery electrodes. Nano Lett 13:3385–3390. https://doi.org/10.1021/nl401729r

25. Liu HJ, Wang XM, Cui WJ, et al (2010) Highly ordered mesoporous carbon nanofiber arrays from a crab shell biological template and its application in supercapacitors and fuel cells. J Mater Chem

20:4223–4230. https://doi.org/10.1039/b925776d

26. Lotfabad EM, Ding J, Cui K, et al (2014) High-density sodium and lithium ion battery anodes from banana peels. ACS Nano 8:7115–7129. https://doi.org/10.1021/nn502045y

27. Ibrahim Abouelamaiem D, Mostazo-López MJ, He G, et al (2018) New insights into the electrochemical behaviour of porous carbon electrodes for supercapacitors. J Energy Storage 19:337–347. https://doi.org/10.1016/j.est.2018.08.014

28. Liu T, Zhang F, Song Y, Li Y (2017) Revitalizing carbon supercapacitor electrodes with hierarchical porous structures. J Mater Chem A 5:17705–17733. https://doi.org/10.1039/c7ta05646j

29. Balakrishnan B, Balasingam SK, Sivalingam Nallathambi K, et al (2019) Facile synthesis of pristine FeS2 microflowers and hybrid rGO-FeS2 microsphere electrode materials for high performance symmetric capacitors. J Ind Eng Chem 71:191–200. https://doi.org/10.1016/j.jiec.2018.11.022

30. Wang B, Chen JS, Wang Z, et al (2012) Green synthesis of nio nanobelts with exceptional pseudo-capacitive properties. Adv Energy Mater 2:1188–1192. https://doi.org/10.1002/aenm.201200008

31. Cheng P, Gao S, Zang P, et al (2015) Hierarchically porous carbon by activation of shiitake mushroom for capacitive energy storage. Carbon N Y 93:315–324. https://doi.org/10.1016/j.carbon.2015.05.056

32. Li Y, Pan J, Wu J, et al (2019) Mesoporous NiCo 2 O 4 nanoneedles@MnO 2 nanoparticles grown on nickel foam for electrode used in high-performance supercapacitors. J Energy Chem 0:167–177. https://doi.org/10.1016/j.jechem.2018.06.009

33. Karunakaran G, Maduraiveeran G, Kolesnikov E, et al (2018) Ascorbic Acid-Assisted Eco-friendly Synthesis of NiCo2O4 Nanoparticles as an Anode Material for High-Performance Lithium-Ion Batteries. Jom 70:1416–1422. https://doi.org/10.1007/s11837-018-2888-y

34. Balasingam SK, Kundu M, Balakrishnan B, et al (2019) Hematite microdisks as an alternative anode material for lithium-ion batteries. Mater Lett 247:163–166. https://doi.org/10.1016/j.matlet.2019.03.058

35. Zhang JN, Liu P, Jin C, et al (2017) Flexible three-dimensional carbon cloth/carbon fibers/NiCo 2 O 4 composite electrode materials for high-performance all-solid-state electrochemical capacitors. Electrochim Acta 256:90–99. https://doi.org/10.1016/j.electacta.2017.10.005

36. Sethi M, Bhat DK (2019) Facile solvothermal synthesis and high supercapacitor performance of NiCo2O4 nanorods. J Alloys Compd 781:1013–1020. https://doi.org/10.1016/j.jallcom.2018.12.143

37. Luo W, Xue H (2019) The synthesis and electrochemical performance of NiCo 2 O 4 embedded carbon nanofibers for high-performance supercapacitors. Fullerenes Nanotub Carbon Nanostructures 27:189–197. https://doi.org/10.1080/1536383X.2018.1538131

38. Guo CX, Yilmaz G, Chen S, et al (2015) Hierarchical nanocomposite composed of layered V2O5/PEDOT/MnO2nanosheets for high-performance asymmetric supercapacitors. Nano Energy 12:76–87. https://doi.org/10.1016/j.nanoen.2014.12.018

39. Marco JF, Gancedo JR, Gracia M, et al (2000) Characterization of the nickel cobaltite, NiCo2O4, prepared by several methods: An XRD, XANES, EXAFS, and XPS study. J Solid State Chem 153:74–81. https://doi.org/10.1006/jssc.2000.8749

40. Kim JG, Pugmire DL, Battaglia D, Langell MA (2000) Analysis of the NiCo2O4 spinel surface with Auger and X-ray photoelectron spectroscopy. Appl Surf Sci 165:70–84. https://doi.org/10.1016/S0169-4332(00)00378-0

41. Roginskaya YE, Morozova O V., Lubnin EN, et al (1997) Characterization of Bulk and Surface Composition of Cox Ni1 -x Oy Mixed Oxides for Electrocatalysis. Langmuir 13:4621–4627. https://doi.org/10.1021/la9609128

42. Kou H, Li X, Shan H, et al (2017) An optimized Al2O3 layer for enhancing the anode performance of NiCo2O4 nanosheets for sodium-ion batteries. J Mater Chem A 5:17881–17888. https://doi.org/10.1039/c7ta01870c

43. Khalid S, Cao C, Wang L, Zhu Y (2016) Microwave Assisted Synthesis of Porous NiCo2O4Microspheres: Application as High Performance Asymmetric and Symmetric Supercapacitors with Large Areal Capacitance. Sci Rep 6:1–13. https://doi.org/10.1038/srep22699

44. Salunkhe RR, Jang K, Yu H, et al (2011) Chemical synthesis and electrochemical analysis of nickel cobaltite nanostructures for supercapacitor applications. J Alloys Compd 509:6677–6682. https://doi.org/10.1016/j.jallcom.2011.03.136

45. Moosavifard SE, Shamsi J, Fani S, Kadkhodazade S (2014) Facile synthesis of hierarchical CuO nanorod arrays on carbon nanofibers for high-performance supercapacitors. Ceram Int 40:15973–15979. https://doi.org/10.1016/j.ceramint.2014.07.126

46. Salunkhe RR, Jang K, Lee SW, Ahn H (2012) Aligned nickel-cobalt hydroxide nanorod arrays for electrochemical pseudocapacitor applications. RSC Adv 2:3190–3193. https://doi.org/10.1039/c2ra01220k

47. Pang H, Zhang B, Du J, et al (2012) Porous nickel oxide nanospindles with huge specific capacitance and long-life cycle. RSC Adv 2:2257–2261. https://doi.org/10.1039/c2ra00949h

48. Ouyang Y, Huang R, Xia X, et al (2019) Hierarchical structure electrodes of NiO ultrathin nanosheets anchored to NiCo 2 O 4 on carbon cloth with excellent cycle stability for asymmetric supercapacitors. Chem Eng J 355:416–427. https://doi.org/10.1016/j.cej.2018.08.142

49. Balamuralitharan B, Karthick SN, Balasingam SK, et al (2017) Hybrid Reduced Graphene Oxide/Manganese Diselenide Cubes: A New Electrode Material for Supercapacitors. Energy Technol 5:1953–1962. https://doi.org/10.1002/ente.201700097

50. Zou R, Xu K, Wang T, et al (2013) Chain-like NiCo2O4nanowires with different exposed reactive planes for high-performance supercapacitors. J Mater Chem A 1:8560–8566. https://doi.org/10.1039/c3ta11361b

51. Panja T, Díez N, Mysyk R, et al (2019) Robust NiCo 2 O 4 /Superactivated Carbon Aqueous Supercapacitor with High Power Density and Stable Cyclability. ChemElectroChem 6:2536–2545.

https://doi.org/10.1002/celc.201900130

52. Cheng Q, Tang J, Shinya N, Qin LC (2013) Polyaniline modified graphene and carbon nanotube composite electrode for asymmetric supercapacitors of high energy density. J Power Sources 241:423–428. https://doi.org/10.1016/j.jpowsour.2013.04.105

53. Shivakumara S, Kishore B, Penki TR, Munichandraiah N (2015) Symmetric Supercapacitor Based on Reduced Graphene Oxide in Non-Aqueous Electrolyte. ECS Electrochem Lett 4:A87–A89. https://doi.org/10.1149/2.0031508eel